Journal of Applied Sciences

ISSN 1812-5654

science alert

ANSInet
an open access publisher
http://ansinet.com

Journal of Applied Sciences 5 (9): 1582-1588, 2005
ISSN 1812-5654

Diagnosis of Shunt Faults in Power Distribution Feeders and Laterals

Yılmaz Aslan
Faculty of Engineering, Dumlupinar University, 43100, Kutahya, Turkey

Abstract: In this study, a digital fault location and monitoring technique using fibre-optics and current sensors for overhead power distribution systems is presented. By using lateral current data transferred through fibre-optic communication lines to the substation, the possibility of multiple fault point locations are eliminated. The technique, based on an interactive approach whereby an assumed fault point is varied systematically until the actual fault point is found, has culminated in a fault locator design that gives a high accuracy for the vast majority of practically encountered system and fault conditions. The effectiveness of this method is verified through Electromagnetic Transients Program (EMTP) simulations.

Key words: Power distribution feeders, fault location, superimposed components

INTRODUCTION

There has been considerable research effort into the development of impedance based digital fault location techniques with a major emphasis on transmission lines and little work has been done in distribution systems[1-4]. Distribution feeders include single phase, two phase and three phase laterals, off a main three-phase primary distribution feeder. In distribution systems, the presence of remote infeed due, for example private generation to improve the system capacity, introduces difficulties to the conventional fault location techniques, particularly those based on apparent impedance methods which make use of current and voltage samples at a single location. Conventional fault location techniques developed to date for distribution systems, do not consider practical interface errors, load estimation errors, shunt faults in laterals and the possible presence of remote source associated with private generation[5-7].

It is generally well known that a conventional fault locator algorithm leads to unacceptable errors in the case of radial distribution feeders with laterals. The fault may be in the main primary distribution feeder or in one of the three phase laterals tapped off from the primary distribution feeder. Moreover, in fault location algorithms based on apparent impedance, occurrence of a fault in the main feeder or in one of the branches may give the same impedance at the substation where measurements are performed and the presence of remote source causes under or over distance measurements[7,8].

In this study with the method of superimposed components[9-11] and using fibre optic communications, shunt faults that may occur in overhead radial power distribution feeders and laterals are analysed. In the algorithm, the type of the fault and fault currents at the fault point are accurately calculated and by using the current and voltage measurements and the data from laterals the exact location of the fault is found.

Location of faults in subfeeders: Figure 1a and b show the voltage and current waveforms recorded by Digital Fault Recorder (DFR) at the substation for a phase (a)-to-earth fault.

In the fault location algorithm, current and voltage samples are continuously monitored at the locator end (end P in Fig. 2) and upon the inception of a fault, a predefined number of voltage and current samples are captured which contain both pre-fault and post-fault information. In the execution of the fault location program, filtered pre- and post-fault voltage and current phasors are obtained through the employment of Discrete Fourier Transform (DFT) filters. Meanwhile the necessary parameters relating to a particular distribution system such as length of the feeder and tap lines, distance between load taps, load and source information etc. are obtained from a database; this data is then used to set up the distribution system model on a computer.

In order to facilitate and expedite the actual location of a fault, the implementation of the fault location algorithm is fully automated; this involves scanning of distribution system at 10 m intervals, initially assuming a fault position at end P. The fault path currents obtained for each assumed fault position are then written into an output file for further inspection. The data is then interrogated automatically in order to ascertain the minimum values of the fault path currents; the point at which this occurs is then the actual fault position as predicted by the fault locator algorithm.

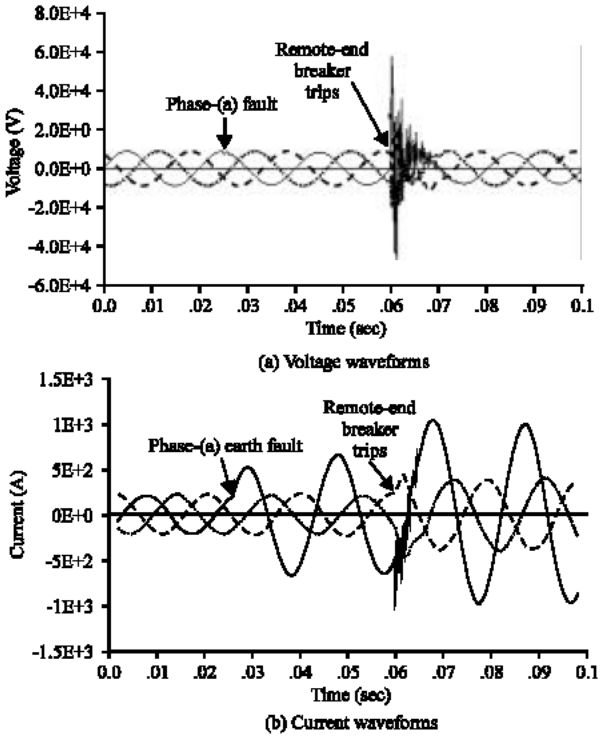

Fig. 1: Phase 'a'-earth fault

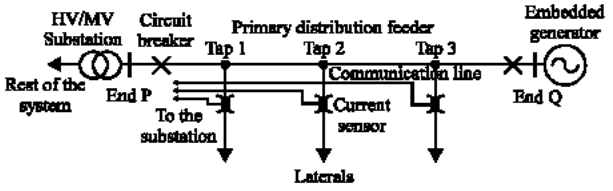

Fig. 2: Distribution system with laterals and embedded generation

The proposed technique, power distribution sub-feeders are equipped with a current sensor in order to classify the faults to the main feeder or to any lateral (Fig. 2). During the fault in a lateral, according to addressed signal received by the main computer at the substation, the pre- and post-fault voltage and current data already captured by the DFR is further processed to update voltage and current values to the faulted lateral. Then by using the voltage and current data the faulted lateral is scanned and the exact location of the fault is found.

In the presence of a remote source connected to the distribution system as shown in Fig. 2, during the shunt fault, it is disconnected from the system instantly to prevent islanding[12]. In post-fault analysis the system is considered as radial.

The theory of superimposed components as applied to a plain feeder: The methodology outlined is based on the principle of determining the superimposed voltage and current values at any assumed fault point from the measured pre- and the post-fault voltage and current data. The superimposed values are simply the difference between the pre- and post-fault steady-state voltage/current signals. The superimposed voltage is than back injected to the feeder at the assumed fault point to check currents in the healthy phases. Only when the fault point is correct do the sound phase(s) injected currents at the fault point attain a zero value. The principle can be best illustrated with reference to simple example as shown in Fig. 3, which is a plain feeder with no laterals.

Assuming a lumped parameter model of the line (this is simply to simplify the explanation, the pre-fault steady-state voltage phasors $V_{F\,a,b,c(ss)}$ at the assumed fault point 'β' related to the measured pre-fault voltage and current phasors ($V_{pa,b,c(ss)}$ and $I_{Pa,b,c(ss)}$) can be expressed as:

$$\left[V_{F_{a,b,c(ss)}(\beta)}\right]=-\beta[Z_{abc}]\left[I_{P_{a,b,c(ss)}}\right]+\left[V_{P_{a,b,c(ss)}}\right] \qquad (1)$$

Where, Z_{abc} is the abc impedance matrix of the feeder (in Ω/unit length). The post-fault voltage phasors at the assumed fault point β can be written as:

$$\left[V_{F_{a,b,c}(\beta)}\right]=-\beta[Z_{abc}]\left[I_{P_{a,b,c}}\right]+\left[V_{P_{a,b,c}}\right] \qquad (2)$$

Where, $I_{P\,a,b,c}$ and $V_{P\,a,b,c}$ are the post-fault line current and voltage phasors at the sending end of the system, respectively. By using the voltage and current data measured at bus P the superimposed voltage phasors at the prospective fault point β are given as:

$$\left[V'_{F_{a,b,c}}(\beta)\right]=\left[V_{F_{a,b,c}}(\beta)\right]+\left[V_{F_{a,b,c(ss)}}(\beta)\right] \qquad (3)$$

Measurements required for a locator, at bus-bar P, comprise the voltage and current phasors that exist before the fault $V_{P_{a,b,c(ss)}}$ and $I_{P_{a,b,c(ss)}}$ and the voltage and current phasors during the fault (before the operation of circuit breakers) $V_{P_{a,b,c(ss)}}$ and $I_{P_{a,b,c(ss)}}$. The superimposed voltage phasors at the end P can be expressed as:

$$\left[V'_{P_{a,b,c}}\right]=\left[V_{P_{a,b,c}}\right]-\left[V_{P_{a,b,c(ss)}}\right] \qquad (4)$$

By injecting the superimposed fault voltages at the assumed fault point 'β', superimposed fault path currents are obtained. The superimposed current phasors at the measuring end P (which are simply the difference between the measured post-fault and pre-fault values) are given by,

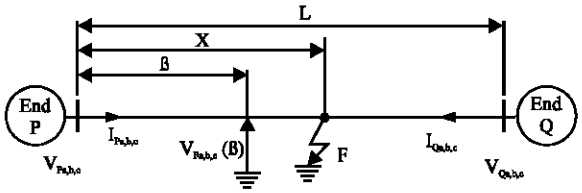

Fig. 3: Faulted plain distribution feeder model

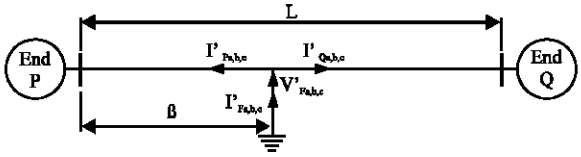

Fig. 4: Injection of superimposed voltages

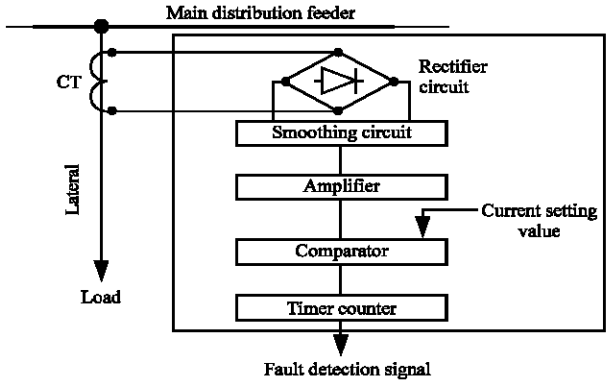

Fig. 5: The schematic of current sensor

$$\left[I'_{P_{a,b,c}}\right] = \left[I_{P_{a,b,c}}\right] - \left[I_{P_{a,b,c(ss)}}\right] \quad (5)$$

With reference to the superimposed system model shown in Fig. 4 these are also the superimposed currents fed into the fault from end P. Again with reference to Fig. 4, the superimposed currents at the remote end Q (which are also the superimposed currents fed into the fault from Q) are given by;

$$\left[I'_{Q_{a,b,c}}\right] = \left[(L-\beta)[Z_{abc}] + [Z_{SR}]\right]^{-1}\left[V'_{F_{a,b,c}}\right] \quad (6)$$

Where, L is the total length of the line, $[Z_{SR}]$ is the impedance matrix representing the remote end source at bus Q and $V'_{F_{a,b,c}}$ the superimposed voltages at the prospective fault point 'β' are obtained from the Eq. 4. The superimposed fault path currents at the assumed fault point 'β' are,

$$\left[I'_{F_{a,b,c}}\right] = \left[I'_{P_{a,b,c}}\right] + \left[I'_{Q_{a,b,c}}\right] \quad (7)$$

In the fault location algorithm, after the fault time inception, the superimposed voltages are computed at the assumed fault point β and then back injected to check the fault path currents in the healthy phase or phases (Fig. 3). The assumed fault point β is shifted in an iterative fashion and when a zero or near to zero value is obtained for the healthy phase or phases, this particular point corresponds to the actual fault point 'X' as shown in Fig. 3.

The current sensing device: In the implementation of the technique an over-current sensing device (Fig. 5) is incorporated in to the algorithm[13]. The device is connected to the laterals through current transformers and it adopts the scheme in which after the input current is rectified and smoothed, it is continuously compared with the setting value of operating current. If the current is higher then the predefined threshold level, the over-current detection signal is sent out via fibre optic cables to the main computer at the substation.

Communication between the substation and sensors: Although within the substation or control centre twisted pair, coaxial cable media alternatives exist, due to its immunity to the electromagnetic disturbances and high capacity optical fibre optic cables are chosen as communication media. For the local area network, star network topology is chosen and by using an active star coupler it will have the same properties as an electrical bus. Bus and star topologies allow somewhat faster communication compared to ring. For data transmission half-duplex data communication system is used which is the most common method for the substation control systems[14].

Fault inception time identification: Before the application of the fault location algorithm any changes in stored current and voltage samples should be identified. In the DFR, after the digitisation stage, the microprocessor continuously executes a monitoring routine. In this process, current and voltage samples from the near end of the distribution line, are measured and stored in the RAM memory of the computer. In the presence of a fault, current and voltage waveforms are distorted and magnitude and phase angle may change with respect to the pre-fault conditions. In this process the first three samples of the second cycle are compared with the corresponding three samples of the previous cycle. Any significant change more than a predefined threshold level indicates the time at which fault has occurred. If these criteria are not satisfied for current samples, the same process is applied to voltage samples[10].

Extraction of voltage and current phasors: As can be seen from the waveforms in Fig. 1, after the fault the

voltage waveforms are distorted with high frequency components while in current waveforms, DC off-set is more prominent. In the fault location algorithm, in order to achieve a high degree of accuracy, after the A/D conversion it is vitally important to extract power frequency voltage and current phasors from the post-fault waveforms which can contain transients ranging from high frequencies down to DC levels. Discrete Fourier Transform (DFT) is very efficient in rejecting high frequency components and effectively attenuates the DC offset[15].

The method used here is based on one cycle of information and the general DFT equation which gives both magnitude and phase of the fundamental phasor $X_{v,i}(\omega)$ is given as:

$$X_{v,i}(\omega)=\left(\frac{2}{N}\right)\sum_{n=0}^{n=N-1}\left[X_{v,i}(n)\{\cos(\omega n\Delta t)-j\ \sin(\omega n\Delta t)\}\right] \quad (8)$$

Where, N shows the number of samples in a cycle, Δt sampling time, ω frequency of phasor to be extracted and $X_{v,i}(n)$, sampled voltage or current waveforms.

Interface: The interface modules comprise of input transformers for voltages and currents and low pass filters. The transformers convert the outputs from the main line Voltage Transformers (VTs) and Current Transformers (CTs) into equivalent voltages (±10 V). The voltage and current values are sampled at 4 kHz and in order to avoid aliasing, a second order Butterworth filter with a cut-off frequency of 1.5 kHz is used. The three phase voltage and current signals are then fed to six sample and hold devices. The outputs from the devices are then passed through a multiplexer and the analogue data is finally converted into binary data by a 12-bit A/D converter that is configured for bipolar analogue inputs between ±10 V. The $\pm 2^{11}$ conversion process leads to a quantisation level of approximately 4.8 mV. After the digitisation stage, the voltage and current data is acquired and stored in a circular buffer in the RAM memory before being printed, processed or transmitted. Usually computer scans the voltage and current samples, storing the data and the oldest information being overwritten.

Derivation of the admittance matrices: Figure 6 shows a typical radial distribution system model with laterals tapped off from the main feeder where, V_P and I_P are voltage and current phasors recorded at end P, V_{Ti} is the voltage at bus i, I_{Li} is the current vector for the lateral i and I_j is the current in the line section j and Z_j is the impedance matrix of that section.

For the calculation of superimposed fault path currents at the assumed fault point, it is necessary to

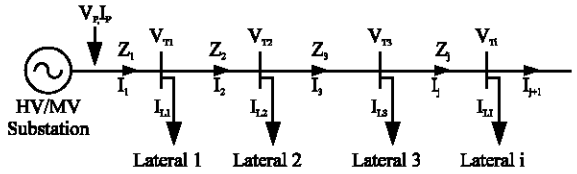

Fig. 6: Distribution system with laterals

calculate the impedance on each side of the assumed fault point in order to force the network. The method of determining the driving impedances is shown by considering a remote end source[10].

Voltages and currents at the prospective faulted lateral: The fault distance algorithm described above assumes that measurements are available at the sending-end of the distribution system. In practice, however, the distribution system is a massive radial network of line segments, with measurements available only at the substation. Hence an estimation procedure is required to determine the voltages and currents at the beginning of each potential faulted lateral based on substation measurements and knowledge of construction configurations. With reference to Fig. 6 the voltage phasors at the load tap i;

$$[V_{Ti}]=[V_P]-\sum_{j=1}^{i}[Z_j][I_j] \quad (9)$$

Where, V_P can be either pre-fault or post-fault voltages, Z_j is the impedance matrix of the main distribution line between two load taps and I_j is the current vector in this line section. The current phasors in line section j may be expressed as;

$$[I_j]=[I_P]-\sum_{i=1}^{j=1}[I_{Lj}] \quad (10)$$

and the pre- and post-fault currents in healthy laterals;

$$[I_{Li}]=[I_j]-[I_{j+1}] \quad (11)$$

During the fault the post-fault currents in the faulted lateral may be stated as,

$$[I_{L_i}]=[I_j]-[V_{T_i}][Y_{ER_i}] \quad (12)$$

where $[Y_{ER_i}]$ is the admittance seen at tap i towards end Q (excluding the admittance of the lateral connected to tap i).

Load and source modelling: In the distribution system application, there will be a mixture of star and delta connected loads terminating a length of lateral. In setting up the load impedance, the variation of load with the time

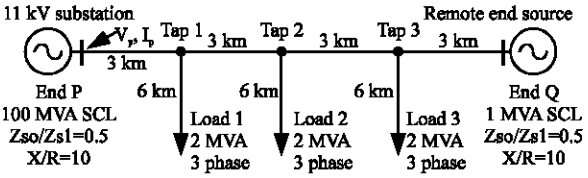

Fig. 7: 11 kV power distribution system

of the day is taken into account and the active power fed to the feeder is approximated from the voltage and current information at the measuring point.

Although the majority of low voltage distribution systems comprise of radial feeders with remote end open, there can be cases where a line section is terminated by a primary substation. The source admittance matrix [Y_{SR}] is defined in terms of the symmetrical short circuit level[10] and ratio of Z_{S0}/Z_{S1}.

Practical considerations: The practical distribution system studied in this work is an 11 kV overhead system with three phase laterals tapped off at various locations from the main feeder as shown in Fig. 7. Since the studies also relate to remote source infeed, the termination of the remote-end with a substation is taken into account. The power frequency is 50 Hz and average earth resistivity is assumed as 100 Ωm. The distribution lines simulated in this work are aluminium–alloy conductors with no earth wires based on horizontal line configuration. In the system loads are considered as series R-L with a typical power factor assumed to be 0.9 lagging. The sources are star connected and the neutral point is earthed with a solid conductor or through impedance.

Results: The effectiveness of the technique developed is tested for different fault locations and types, fault resistance, source capacities and fault cycle.

Effect of fault location: Table 1 shows the effect of fault type for faults on laterals on the fault locator's accuracy for a 11 kV system as shown in Fig. 7. Faults were created in each lateral at 3 km. As can be seen from the results, the fault locator gives an inherently high accuracy for faults created in laterals. However there is a small decrease in accuracy for the phase-phase faults. This is due to the fact the superimposed fault path currents computed for line-line faults are relatively lower and this leads to more quantization and computational errors.

Effect of fault resistance: The effect of fault resistance was also tested on the aforementioned distribution system for different fault resistances. The fault locator gives an inherently high accuracy in the presence of fault

Table 1: Effect of fault type on locator's accuracy (R_f=2Ω)

	Lateral 1		Lateral 2		Lateral 3	
Fault type	Estimated distance (km)	Error (%)	Estimated distance (km)	Error (%)	Estimated distance (km)	Error (%)
a-e	3.13	2.16	3.20	3.33	3.23	3.23
a-b-e	2.80	3.33	3.10	1.65	3.30	3.30
a-b	3.00	0.00	2.70	5.00	2.50	2.50

Table 2: Effect of fault resistance on locator's accuracy

(R_f)	Lateral 1		Lateral 2		Lateral 3	
Fault resistance (Ω)	Estimated distance (km)	Error (%)	Estimated distance (km)	Error (%)	Estimated distance (km)	Error (%)
2.0	3.13	2.16	3.20	3.33	2.0	3.23
20.0	3.28	4.67	3.15	2.50	20.0	3.30
50.0	3.53	8.83	2.92	1.33	50.0	3.55

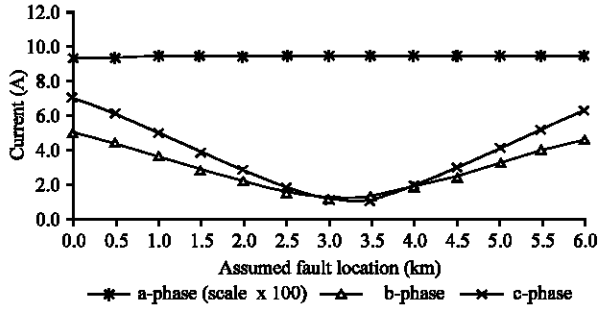

Fig. 8a: Fault path currents for 'a'-phase-earth fault (R_f=2 Ω)

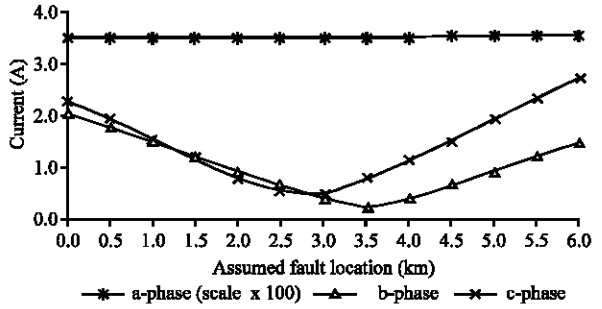

Fig. 8b: Fault path currents for 'a'-phase-earth fault (R_f=20 Ω)

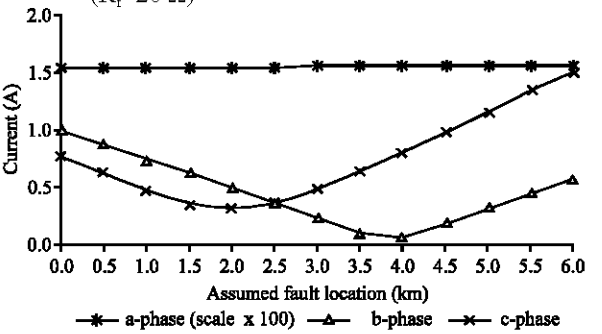

Fig. 8c: Fault path currents for 'a'-phase-earth fault (R_f=50 Ω)

resistance for faults on laterals (Table 2). However, there is a small decrease in accuracy for single-phase earth faults especially when the fault resistance exceeds 50 Ω. The effect of fault resistance is not studied for phase-phase faults because in practice the fault resistance for such type of faults rarely exceeds about 1 Ω.

Figure 8a-c shows the effect of fault resistance on the accuracies attained for the distribution system shown in Fig. 7, subjected to an 'a'-phase-earth fault created at the 3 km of the second lateral for typical fault resistance values of 2, 20 and 50 Ω, respectively.

It is evident that with an increase of fault resistance, the fault path currents get attenuated and the change in the healthy phase fault path currents at the actual fault point gets less discrete as a consequence. This can directly attributed to the fact in the presence of fault resistance, for all phases I'_P that is fed into the fault from end P decreases; the superimposed voltage V'_F at the actual fault point decreases with an increase in fault resistance; this results in a lover I'_Q that is fed into the fault from end Q for all phases. Finally, the I'_F which is the total of superimposed currents fed into the fault at the assumed fault point decreases and in this case the effect of computational and quantisation errors are accentuated.

It can be concluded from the foregoing results presented that the overall performance attained is significantly superior to that achieved with conventional techniques, particularly those based on impedance to fault measurements, which give rise to unacceptably large errors in the presence of fault resistance[8].

Effect of source capacity: Although the actual fault location algorithm is independent of source capacity at the end P, it is important to ascertain if the location estimation is significantly influenced by changes in source at the end P. Table 3 summarises effect of remote source capacity on accuracy for various types of faults for the system shown in Fig. 7. The source capacity at end Q is varied from 1 MVA up to 100 MVA and various types of faults are created on lateral 3 at 3 km. From the results it is seen that for same fault types similar errors are attained under different remote source capacities. This can be directly attributed to the fact that under the fault, remote end source is disconnected hence the currents fed to the fault from end Q is virtually eliminated.

Effect of fault cycle: In the fault location algorithm, the DFT technique ignores the first cycle of post-fault data since the transients are most prominent during this period. However, there can be situations particularly under high-speed fault clearance when only one cycle of fault information is available to the fault location after the remote end breaker opening. In this case it is no longer possible to ignore the first cycle of fault information and all the post-fault information must be taken into account. A comparison of accuracies attained between utilising the first and second cycle of data following a fault for various types of fault is investigated. The results clearly show that for single-phase-earth and double-phase faults, the accuracy is not significantly affected. In the case of phase-phase faults, however, the accuracy is slightly decreased when the first cycle of information is utilised. This can be attributed to the fact that when the first cycle of fault information is used there is still some DC off-set and distortion present both in voltage and current waveforms. This effectively means that the extraction of the fundamental phasors via the DFT filter causes some errors.

Table 3: Effect of remote source capacity

Fault type	(R_f) Fault resistance (Ω)	SCL 10 MVA		SCL 100 MVA	
		Estimated distance (km)	Error (%)	Estimated distance (km)	Error (%)
a-e	2.0	3.25	4.15	3.28	4.65
a-e	20.0	3.30	5.00	3.33	5.50
a-b-e	2.0	3.30	5.00	3.30	5.00
a-b	2.0	2.50	8.33	2.50	8.33

CONCLUSIONS

The fault location algorithm is based on utilising superimposed phase signals and special filtering techniques are utilised to accurately extract the fundamental phasors from the measured fault signals. The results presented also show the locator's robustness to large errors in the estimation of load taps and remote source capacity.

Although the algorithm has been tested using CAD techniques, emphasis is placed on examining its performance using data as though it were captured through actual fault recorders; it is clearly demonstrated that with this approach, the algorithm retains its high accuracy in the presence of errors introduced by transducers and hardware, the errors attained being less than about 9% for the majority of system and fault conditions studied.

The algorithm is implemented on a typical 11 kV overhead distribution system with horizontal line configuration. In this system presence of loads tapped off from the main feeder throughout the system are taken into account and also faults on systems with remote infeed are studied in details. The performance of the technique described herein is also examined for faults on the distribution system with remote-end infeed. It is shown that in comparison to the results attained for the open ended radial feeder system the presence of remote infeed improves the accuracy slightly. This is a significant advantage and in marked contrast to conventional fault location algorithms, particularly those

based on impedance measurements, whose accuracy deteriorates in the presence of any remote infeed.

In this technique, rather than total values of currents and voltages superimposed components are used. Thus the effect of preloading conditions and source impedance on accuracy is virtually eliminated. Hence the proposed algorithm does not require any local source impedance setting and therefore any inaccuracies (or changes) in source parameters are of no consequence to this technique. This is a significant advantage over other techniques, since in distribution systems source capacity.

REFERENCES

1. Erikson, L., M.M. Saha and G.D. Rockefeller, 1985. An accurate fault locator with compensation for apparent reactance in the fault resistance resulting from remote-end infeed. IEEE Transactions on Power Apparatus, Sys., PAS-104: 424-435.
2. Takagi, T., Y. Yamakoshi, M. Yamura, R. Kondow and T. Matsushima, 1982. Development of a new type fault locator using the one-terminal voltage and current data. IEEE Transactions on Power Apparatus, Sys., PAS-101: 2892-2898.
3. Sacdev, M.S. and R. Agarwal, 1986. A technique for estimating transmission line fault locations from digital impedance relay measurements. IEEE Trans. Power Sys., PWRD-1: 442-451.
4. Lawrance, D.J. and D.L. Waser, 1988. Transmission line fault location using digital fault recorders. IEEE Trans. Power Deliv., 3: 496-502.
5. Girgis, A.A., M. Fallon, M. Christopher and D.L. Lubkeman, 1993. A fault location technique for rural distribution feeders. IEEE Trans. Indus., Applications, 29: 1170-1175.
6. Das, R., M.S. Sachdev and T.S. Sidhu, 1995. A technique for estimating location of shunt faults on distribution lines. Proc. IEEE, Wescanex'95.
7. Zhu, J., L.L. David and A.A. Girgis, 1996. Automated fault location and diagnosis on electric power distribution feeders. IEEE Winter Meeting.
8. Cook, V., 1986. Fundamental aspects of fault location algorithm used in distance protection. IEE Proc., 5: 359-365.
9. Aggarwal, R.K., Y. Aslan and A.T. Johns, 1997. A new concept in fault location for overhead distribution systems using superimposed components. IEE Proc. C, May, 144: 309-316.
10. Aslan, Y., R.K. Aggarwal and A.T. Johns, 1995. Fault location in overhead distribution systems using superimposed components. 30th Univ. Power Eng. Conf., 1995 Univ. Greenwich, UK., pp: 184-187.
11. Johns, A.T., P.J. Moore and R. Whittard, 1995. New technique for the accurate location of earth faults on transmission systems. IEE Proc. C, March, 142: 119-127.
12. Redfern, M.A. and O. Usta, 1995. A new microprocessor based islanding protection algorithm for dispersed storage and generation units. IEEE Trans. Power Deliv., 10.
13. Kakimoto, H., T. Hayashi, H. Handa, K. Yukihira, Y. Okamura and N. Odaka, 1995. Development of automatic fault point locating and sectional isolating system for power distribution line. Elect. Eng. Japan, 115: 75-87.
14. Moore, P.J., 1997. Power system protection. Digital protection and signalling. Inst. Elect. Eng., 4.
15. Aggarwal, R.K., D.V. Coury, A.T. Johns and A. Kalam, 1993. A practical approach to accurate fault location on extra high voltage teed feeders. IEEE Trans. Power Deliv., 8: 874-883.